

Optimization Strategies for Multi-Aperture SAR Imaging With High Performance

Nicolas Gebert (nico.gebert@dlr.de), Gerhard Krieger, Alberto Moreira

Microwaves and Radar Institute, German Aerospace Center (DLR), 82234 Wessling, Germany

Abstract - Multi-aperture synthetic aperture radar (SAR) systems enable high performance SAR imaging thus meeting the rising demands of future remote sensing applications that conventional SAR cannot fulfill. To provide constant performance even in case of a non-uniformly sampled data array in azimuth caused by a non-optimum pulse repetition frequency (PRF), an appropriate coherent processing of the individual aperture signals is needed. An innovative multi-aperture reconstruction algorithm for such a ‘digital beamforming on receive’ was presented and investigated in [1]-[6]. This paper continues with a system design example to demonstrate the algorithm’s capability for high performance imaging. Further, innovative strategies and extended system architectures allowing for optimizing the system performance are introduced and their effectiveness is shown by simulation results. In this context, the theoretical characterization of the impact of the processing on the NESZ is extended to the new concepts.

I. INTRODUCTION

Remote sensing of the earth demands increasingly for sensors that are capable of continuous global coverage and, in addition, provide detailed imagery. This can be achieved by new system concepts employing multi-channel SAR systems where the receiving antenna is either split into multiple sub-apertures or even distributed on multiple platforms. Different approaches are listed in [1]. If the apertures are arranged in azimuth, optimum system performance is obtained if the relation between sensor velocity v and the along-track offsets Δx of the N sub-apertures result in equally spaced effective phase centers thus leading to a uniform spatial distribution of the received signal samples. In a single platform system, this translates to an optimum PRF :

$$PRF_{opt} = \frac{2 \cdot v}{N \cdot \Delta x} \quad (1)$$

In case of a non-optimum PRF , the gathered samples are spaced non-uniformly what requires an additional processing of the multi-aperture azimuth signals before conventional monostatic focusing algorithms are applied. The purpose of this processing is to combine the N channels, each of bandwidth $N \cdot PRF$ but sub-sampled with PRF , to obtain a signal effectively sampled with $N \cdot PRF$ thus fulfilling the Nyquist criterion. As a solution to this digital beamforming, a multi-aperture reconstruction algorithm that is based on solving a system of linear equations to unambiguously recover the formerly aliased azimuth spectrum has shown great potential. A detailed derivation and investigation can be found in [1]-[5]. In particular, the multi-aperture reconstruction approach turns out to be the most suitable of several investigated algorithms to mitigate the negative effects of a non-optimum PRF on key performance figures [6], [7]. In Section II a system design

example for high performance imaging will be presented to demonstrate the algorithm’s capability. Nevertheless, large deviations from the optimum PRF entailing strong non-uniform sampling still cause an unwanted degradation of the performance and thus restrict the range of application. Hence, to extend the possible range of PRF , optimized processing strategies and advanced system architectures are required that will be discussed in Sections III-VI.

II. REFERENCE SYSTEM

In the following, the basic mission performance requirements and parameters of the investigated multi-aperture SAR system are summarized in Table I and II, respectively. As the focus is on azimuth processing, only the relevant parameters are listed. For a complete derivation of the system design and a detailed analysis of the system and its optimization, refer to [7].

Performance Requirement	Symbol	Value
Swath-width	L_{sw}	100 km
Coverage (Incident angle)	Θ_i	20° - 55°
Geometric Resolution (Azimuth, Range)	δ_{az}, δ_{rg}	≤ 1 m
Azimuth Ambiguity Suppression	$AASR_N$	≤ -21 dB
Noise equivalent sigma zero	$NESZ$	≤ -19 dB

TABLE I. Requirements of the high-performance SAR system

System Parameters	Symbol	Value
Carrier wavelength	λ	3.1 cm
Orbit height	h_s	580 km
Rx Sub-apertures in azimuth	N	7
Rx Sub-aperture length in azimuth	$d_{a,rx}$	1.6 m
Required PRF range	PRF	1240 - 1470 Hz
Tx antenna in azimuth	$d_{a,tx}$	3.0 m
Sensor velocity	v	7560 m/s
Processed azimuth bandwidth	B_D	7.6 kHz
Receive antenna height in elevation	H_a	2 m
Maximum Receive antenna gain	G_{rx}	53.8 dB
Transmit peak power	P_{tx}	5 kW
Losses (atmospheric, system, receiver noise, 2-way)	L	5.7 dB
Azimuth loss	L_{az}	3.05 dB

TABLE II. System parameters of the investigated SAR system

A. NESZ

The noise power in the reconstructed data (p_n) with respect to the noise power in a single receiving element at the point of reception ($p_{n,el}$) can be determined by (2), where $P_j(f)$ represent the filter functions of the processing network [3]. G and F describe power gain and noise figure of the LNA in the receiver, respectively. In order to characterize the noise power in the focused image ($p_{n,BD}$), an additional lowpass filter of bandwidth B_D has to be taken into account (cf. (3)). The resulting curves for the investigated system are shown in Fig. 1. One observes that especially for PRF values below 1240 Hz the rise of the noise power becomes unacceptably strong.

$$\frac{p_n}{p_{n,el}} = G \cdot F \cdot \sum_{j=1}^N \mathbf{E} \left[|P_j(f)|^2 \right] \quad (2)$$

$$\frac{p_{n,B_D}}{p_{n,el}} = G \cdot F \cdot \sum_{j=1}^N \mathbf{E} \left[|P_j(f)|^2 \cdot \text{rect} \left(\frac{f}{B_D} \right) \right] \quad (3)$$

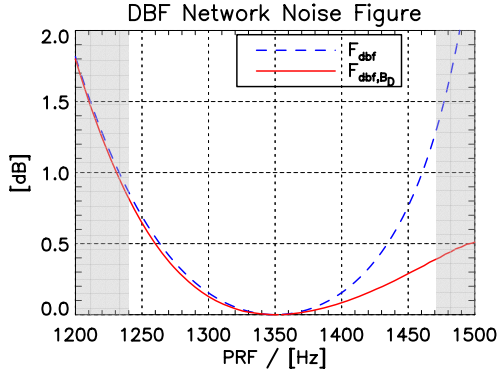


Fig. 1. Characteristic of the *SNR degradation vs. PRF* due to the signal reconstruction considering the processed Doppler bandwidth of 7.6 kHz (solid red) and for the whole bandwidth (dashed blue). The *PRF* region of interest is limited by the shaded areas.

Considering the impact of the processing network on the signal power and combining it with (2) and (3), one obtains an expression for the noise figure of the beamforming network, F_{abf} , dependent on the *PRF*. This expression can be used to extend the standard expression for the *NESZ* [8] by inserting the respective F_{abf} for each of the swaths. Inserting the values for the losses given in Table II, the system *NESZ* is given by Fig. 2.

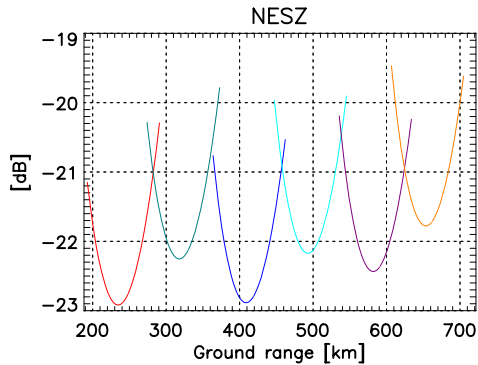


Fig. 2. *NESZ vs. ground range*. 6 swaths of 100 km length.

B. Ambiguous Energy Suppression

Fig. 3 shows the azimuth ambiguous energy suppression of distributed targets ($AASR_N$) vs. *PRF* for different processing methods. It is observed that only the multi-aperture reconstruction (solid red line) and the nearly identical null-steering provide sufficient suppression over the whole range of *PRF* while all other methods fail except around the uniform *PRF* of 1350 Hz. The azimuth resolution is slightly below 1 m.

III. OPTIMIZATION POTENTIALS

In this Section, origin of aliasing and receiver noise and their propagation through the beamforming network are analyzed. Then strategies are developed for improving the *NESZ* and the ambiguity suppression while keeping

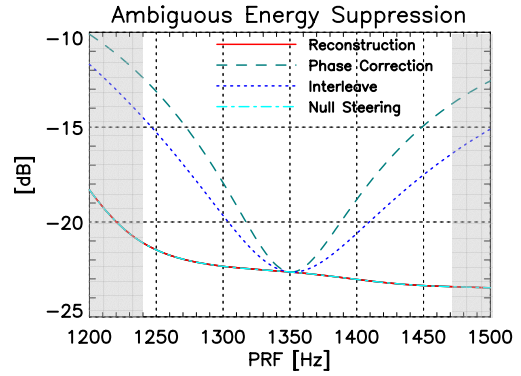


Fig. 3. Azimuth ambiguity suppression achieved by reconstruction algorithm (solid red) compared to phase correction (dashed green) [9], simple interleave of samples (dotted blue) and pattern null-steering (dashed light blue) [10].

the resolution at a constant level thus optimizing the SAR system performance. Specific methods for optimization follow in the subsequent Sections.

The ambiguous energy in the signal after reconstruction is determined by Doppler frequencies $|f_D| > PRF \cdot N/2$ within the joint antenna characteristic. In the beamforming network, this ambiguous energy is weighted and possibly amplified by the power spectral densities of the filter functions $P_{jm}(f)$. In the same way, the receiver noise power is subject to a possible amplification by these filters while the signal energy is preserved, what results in a degraded *NESZ*. Hence the first aspect is to minimize the ambiguous frequencies by optimally confining the joint antenna pattern to the desired band by an appropriate pattern tapering on transmit and receive. Secondly, the amplification of existing ambiguous and noisy contributions by the power spectral densities of the filters $P_{jm}(f)$ is to be minimized, what is equivalent to ensuring a spatial sampling as uniform as possible. As in general the system *PRF* is set by the timing, this requires the adaptation of the effective phase centers on transmit and/or receive to influence the sampling.

IV. PATTERN TAPERING ON TRANSMIT

Pattern tapering on transmit offers a simple tool to effectively cancel ambiguous Doppler frequencies. The po-

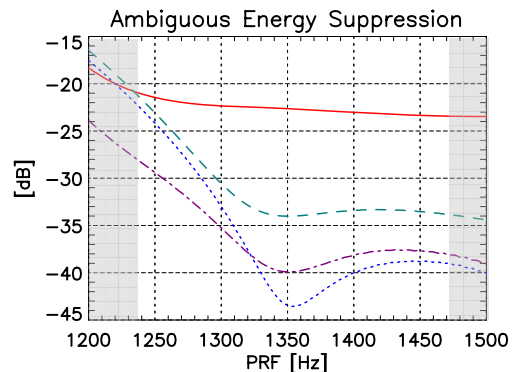


Fig. 4. Suppression of azimuth ambiguities vs. *PRF* for different transmit antenna sizes and patterns. $\sin(f)/f$ pattern for an aperture size of 3 m (solid red) in comparison to a 4 m antenna with a $\cos(f)$ pattern (dashed green), a 5 m antenna with a $(\sin(f)/f)^2$ pattern (dotted blue) and an approximate rectangular pattern (dotted dashed violet) for a 11.2 m antenna.

tential is demonstrated by evaluating the $AASR_N$ of the system of II with different combinations of transmit antenna dimensions and excitations. Fig. 4 summarizes the results that show a clear improvement for higher PRF values. However, to provide an improvement in suppression also for lower PRF values, a larger transmit antenna is necessary. The best cancellation of the spurious spectral components is achieved by the unconventional but quasi-optimum - as it approximates a rectangular pattern - $\sin(x)/x$ excitation in combination with an antenna length equal to the receive antenna. Note that all scenarios show a resolution below 1 m ($B_D = 7.6$ kHz).

V. PHASE CENTER ADAPTATION ON TRANSMIT

In a further step, one can think of advanced concepts of transmit antenna architectures in azimuth, that allow for adaptively varying the transmit phase center from pulse to pulse by using only defined parts of a large antenna. This enables a phase center position travelling over the antenna from pulse to pulse thus compensating for a non-optimum PRF . By choosing the direction of the sliding phase center along or against the flight direction, it is possible to adjust the spatial sampling resulting from too high or too low PRF values, respectively. The PRF range that can be compensated is determined by the maximum displacement of the phase center, while the fine-tuning ability of the position, i.e. the “step size” of the phase center from pulse to pulse, depends on the distance between single transmit elements. Note that a shift of the phase center from one end of the antenna to the other is necessary every time it has reached its outermost position. In the case of a PRF that is too high this requires combining or even skipping some samples that might overlap while in the case of a PRF that is too low this results in missing samples, as a small gap occurs when the phase center is switched.

As a further example in the same context, more sophisticated techniques based on digital waveform encoding on transmit have to be mentioned, as they offer various and powerful opportunities to push the system performance even further [11].

VI. CASCADED BEAMFORMING NETWORKS

The following Sections address the potential strategies of system optimization arising on receive. In this context cascaded beamforming networks offer great possibilities to adaptively improve the system performance. The basic idea is to extend the system by a second stage that is used for digital or analogue pre-processing of the multi-aperture SAR signals before the reconstruction filter network is passed (cf. Fig. 5). The additional network enables an individual and reconfigurable weighting and combination of the receiving elements’ signals. This allows for the flexible formation of N “virtual” output channels j , which represent the input signals for the succeeding reconstruction filter network. The weights w_{ij} of the input signals may vary from sub-aperture to sub-aperture and from channel to channel. This enables “using” the signal of a certain sub-aperture in more than one of the virtual channels resulting in a spatial overlap of these channels. The contribution of the signal of element i to the channel j is described by the complex coefficient $w_{ij}(f)$.

This processing architecture enables to flexibly adjust

the number and position of the virtual samples to the actual system PRF by combining the respective receiving elements by the pre-processing network [6]. Hence, non-uniform sampling and consequently the amplification of ambiguous energy and noise can be reduced. In addition, the choice of the weights $w_{ij}(f)$ allows for implementing pattern tapering on receive to suppress ambiguities or increase the antenna gain and hence the signal power. The way of weighting and combining the two stages offers wide flexibility regarding the effective sampling ratio, the spatial sampling and the receiving pattern. Therefore, the system setting underlies a trade-off with respect to the performance parameters as $AASR_N$, resolution and $NESZ$.

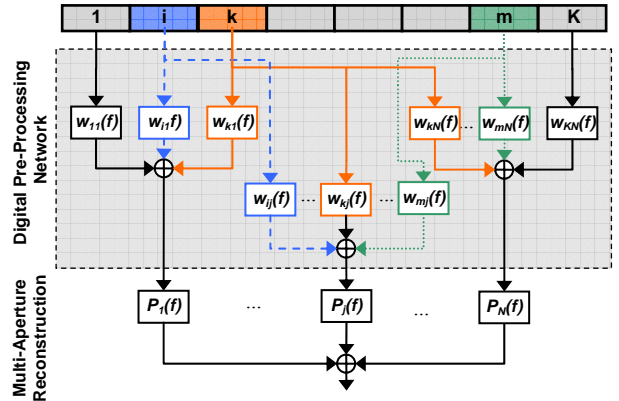


Fig. 5. Cascaded networks: **Digital or Analogue pre-processing stage** followed by reconstruction of N optimized channels with mutual overlap of adjacent beam-steering groups.

Due to the modified processing, the noise figure of the beamforming network changes and the expressions (2) and (3) have to be extended to the cascaded structure. In contrast to a mere digital beamforming network the mutual correlations introduced by the pre-beamshaping have to be considered. Assuming a lossless weighting network and mutually uncorrelated noise, the output noise powers in the data ($p_{n,c}$) and the image ($p_{n,c,BD}$) are given by (4) and (5), respectively. Further, to determine the noise figure of the cascaded network, the impact of the first processing stage on spectral shape and power of the input signal has to be taken into account.

$$\frac{p_{n,pb}}{p_{n,el}} = G \cdot F \cdot \sum_{i=1}^K \mathbf{E} \left[\left| \sum_{j=1}^N P_j(f) \cdot w_{ij} \right|^2 \right] \quad (4)$$

$$\frac{p_{n,pb,BD}}{p_{n,el}} = G \cdot F \cdot \sum_{i=1}^K \mathbf{E} \left[\left| \sum_{j=1}^N P_j(f) \cdot w_{ij}(f) \cdot \text{rect} \left(\frac{f}{B_D} \right) \right|^2 \right] \quad (5)$$

A. Digital Pre-Processing

Firstly, consider a digital pre-processing stage after amplification, down-conversion, digitization and storage of the signals. Note that in this case, all processing is applied a-posteriori and consequently the system setting can be reconfigured arbitrarily to focus on another parameter of interest. On the other hand, the number of individual antenna elements is limited by the available data storage capacity.

The potential of such a cascaded beamforming approach is demonstrated with a system example in the fol-

lowing. Consider the system of Section II, but to be operated in an enlarged PRF range from 1150 Hz to 1550 Hz. As Fig. 1 indicates, the noise figure of the reconstruction network becomes too worse for PRF values below 1240 Hz. Consequently the sub-aperture length is increased to 1.75 m in order to reduce the optimum PRF to ~ 1230 Hz. Further, a slightly increased aperture antenna on transmit of 3.15 m is required to ensure a sufficient ambiguity suppression. In this case, the noise figure of the reconstruction network shows sufficiently low values up from 1150 Hz, but yields unacceptably high values for PRF values higher than 1350 Hz (cf. Fig. 6, solid red line). To operate the system in these PRF ranges, the processing is extended to a cascaded network. In the first stage the signals of two adjacent sub-apertures, respectively, are combined yielding six mutually overlapping output channels that are processed by the multi-aperture reconstruction algorithm. This causes the optimum PRF to be shifted up to 1440 Hz.

The weighting functions $w_{ij}(f)$ are chosen to maximize the signal power. They effectuate a steering of the maximum of the joint antenna characteristic for every $f \in [-B_D/2, B_D/2]$ in the direction corresponding to that frequency. As a consequence, the beamwidth of the first stage's output signal is defined by the single element length, while the gain is determined by the number of channels that are combined. Considering this rise in signal amplitude gain by a factor of 2 and taking into account the reduced number of channels, this yields an increased peak power of 4.68 dB. Further, mutual correlations caused by partly overlapping channels and the reduced effective sampling ratio cause the noise floor to rise by 4.3 dB compared to the optimum value when conventionally operating the system (cf. (4), (5)). Finally this results in an improvement of the noise figure of 0.38 dB when comparing the values at the respective optimum $PRFs$ (cf. Fig. 6, dashed blue line).

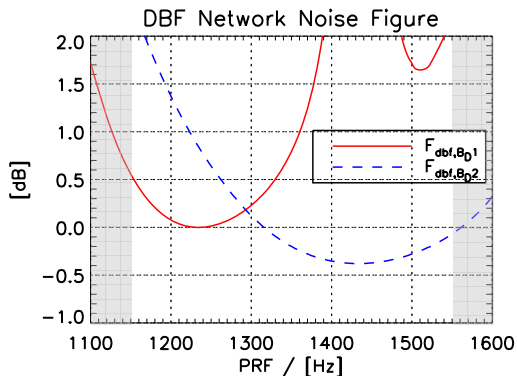


Fig. 6. Noise figures for cascaded beamforming case (dashed blue) compared to conventional DBF (solid red), normalized to the optimum value of the conventional case.

Regarding the $NESZ$, the enlarged antenna dimensions entail increased azimuth losses L_{az} of 3.35 dB compared to 3.05 dB in the reference system of Section II. In return, the larger antennas result in an increased gain of 0.59 dB. Hence, improving the original $NESZ$ of Fig. 2 by ~ 0.3 dB and applying the respective noise figures of Fig. 6 instead of Fig. 1 yields the new $NESZ$.

Next, the ambiguous energy suppression of the system

is investigated and the results are presented in Fig. 7. The red line shows the suppression of the original system that is improved by the adapted beamforming above 1340 Hz (dashed blue line). Due to the reduced effective sampling, this curve starts only at $PRF=B_D/6$. In combination with Fig. 6, one concludes that the conventional approach is suitable for a PRF values up to 1290 Hz, while the cascaded beamforming is favourable above 1340 Hz. In between, the focus can be turned to the $NESZ$ by choosing the cascaded structure or to optimize the $AASR_N$ by applying the conventional approach. The resolution of both approaches is 1.04 m what is slightly above the reference case of II due to the enlarged apertures.

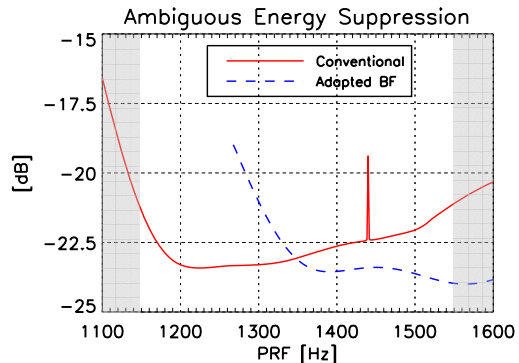


Fig. 7. $AASR_N$ for adapted beamforming (dashed blue) compared to conventional DBF (solid red).

B. Analogue Pre-Beamshaping on Receive

Similar to the method presented before, the pre-processing stage can also be applied to the analogue multi-aperture RF signals. The main difference is an antenna allowing for a larger number of independent elements as the signals are weighted and combined before digitization and storage (cf. Fig. 5). This offers more flexibility in terms of pattern tapering and adjusting the phase centers but disallows a complete a-posteriori processing.

To demonstrate the potential of this “pre-beamshaping on receive” we consider again the modified system presented in Section VI.A, but assume each sub-aperture to consist of a large number of individual elements. Again, a reconfiguration of the pre-beamshaping network is necessary to avoid the unacceptably noise figure above 1350 Hz (cf. Fig. 6, solid red line). In the present case, mutually overlapping sub-apertures of 2.625 m length are formed, resulting in a decreased phase center spacing that corresponds to a new optimum PRF of 1346 Hz. In order to keep the beamwidth of the receiving pattern constant and to suppress its sidelobes, a cosine taper is applied to each of the sub-apertures. The respective noise figure is given in Fig. 8 (dashed blue line) and it takes into account the impact of the sub-aperture dimension and taper on noise power and signal peak power.

Regarding the $NESZ$, an additional azimuth loss of 0.2 dB occurs when switching from conventional operation to pre-beamshaping due to the enlarged sub-aperture length. But as Fig. 8 shows, it is compensated by the better noise figure for a PRF above ~ 1205 Hz. The $NESZ$ of this system can be deduced from the $NESZ$ derived in VI.A taking into account the modified noise figure of Fig. 8.

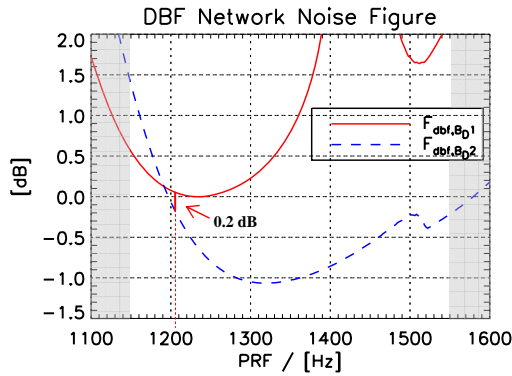


Fig. 8. Noise figure of the conventional digital beamforming network (solid red) and the cascaded network (Pre-Beamshaping) (dashed blue).

Finally, the $AASR_N$ of the modified system is investigated. With pre-processing network, the suppression becomes better for PRF values above ~ 1205 Hz (cf. Fig. 9, dashed blue line). In combination with the results for the noise figure, it is hence favourable to apply the pre-beamshaping up from this PRF . For higher PRF values, the suppression is clearly improved due to reduced sidelobes of the receive pattern and minimized amplification of the ambiguous energy caused by the adapted phase centers. Concerning the resolution, a negligible degradation to 1.03 m is observed, both for conventional and pre-beamshaping system operation.

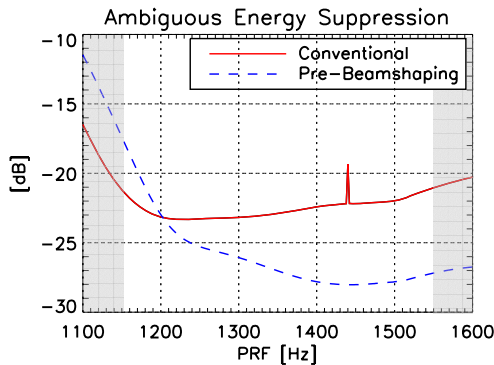


Fig. 9. $AASR_N$ vs. PRF for pre-processing of the signal by a Pre-Beamshaping network (dashed blue) compared to the conventional digital beamforming case (solid red).

VII. SUMMARY

The paper demonstrated the capabilities of the multi-aperture reconstruction algorithm to enable high performance SAR imaging by means of an example system designed to image a swath of 100 km with a geometric resolution of 1 m. Simulation results, including a comparison with alternative processing methods, showed that only the multi-aperture reconstruction algorithm and the very similar null-steering technique provide high resolution and efficient ambiguity suppression even in case of a non-uniformly sampled synthetic aperture. Nevertheless, a large offset from the optimum PRF may result in a degraded $NESZ$ and rising residual azimuth ambiguities as the noisy and aliased components of the input signal are increasingly amplified by the processing network with increasing non-uniform sampling of the azimuth signal.

Hence, the reduction of perturbations in the input signal and the adaptation of the spatial sampling to the imposed PRF were identified as optimization strategies.

Concerning the reduction of perturbations, pattern tapering on transmit and by pre-beamshaping on receive networks showed to be well suited to enforce the limitation of the Doppler spectrum thus reducing azimuth ambiguities. Regarding the spatial sampling, cascaded beamforming networks on receive were introduced and their capability demonstrated to adaptively and flexibly adjust the number and position of the effective phase center thus ensuring the required system performance over a wider PRF range. In this context, the theoretical characterization of the network noise figure was extended to the class of cascaded beamforming systems. Besides, an advanced transmit architecture enabling an adaptive pulse-to-pulse adjustment of the transmit phase center to compensate for non-uniform sampling was established.

The focus of future work is turned to the application of the ScanSAR and TOPS-SAR principle in multi-aperture systems to enable ultra-wide swaths. One aspect currently under investigation is the strong dependency of the beamforming network noise figure on the Doppler sub-band. Hence, different sub-spectra of different targets in a burst mode possibly entail a large variation of the $NESZ$. So, even in the TOPS-SAR mode, this may result in a scalloping-like effect, while in ScanSAR operation the scalloping can be further increased. Such effects can be mitigated by a novel Multi-Beam Burst Mode (MBBM) operation which enables the unambiguous imaging of an ultra-wide swath with high azimuth resolution while keeping the antenna structure compact [12].

REFERENCES

- [1] G. Krieger, N. Gebert, A. Moreira, *Unambiguous SAR Signal Reconstruction from Non-Uniform Displaced Phase Centre Sampling*, IEEE Geoscience and Remote Sensing Letters, vol. 1 (4), 2004
- [2] G. Krieger, N. Gebert, A. Moreira, *SAR Signal Reconstruction from Non-Uniform Displaced Phase Centre Sampling*, IGARSS 2004, Anchorage, Alaska.
- [3] N. Gebert, G. Krieger, A. Moreira, *SAR Signal Reconstruction from Non-Uniform Displaced Phase Centre Sampling in the Presence of Perturbations*, IGARSS 2005, Seoul, Korea.
- [4] N. Gebert, G. Krieger, A. Moreira, *High Resolution Wide Swath SAR Imaging – System Performance and Influence of Perturbations*, IRS 2005, Berlin, Germany.
- [5] N. Gebert, G. Krieger, A. Moreira, *High Resolution Wide Swath SAR Imaging with Digital Beamforming – Performance Analysis, Optimization, System Design*, EUSAR 2006, Dresden, Germany.
- [6] N. Gebert, G. Krieger, A. Moreira, *Digital Beamforming for HRWS-SAR Imaging – System Design, Performance and Optimization Strategies*, IGARSS 2006, Denver, Colorado.
- [7] N. Gebert, G. Krieger, A. Moreira, *Digital Beamforming on Receive: Techniques and Optimization Strategies for High Performance SAR Imaging*, submitted to IEEE Trans. on Aerospace and Electronic Systems, 2007.
- [8] J. Curlander, R. McDonough, *Synthetic Aperture Radar - Systems and Signal Processing*, J. Wiley & Sons, 1991.
- [9] M. Younis, C. Fischer, W. Wiesbeck, *Digital Beamforming in SAR systems*, IEEE Trans. on Geoscience and Remote Sensing, vol. 41 (7), 2003
- [10] H. Li, H. Wang, T. Su, Z. Bao, *Generation of Wide-Swath and High-Resolution SAR Images From Multichannel Small Spaceborne SAR System*, IEEE Geoscience and Remote Sensing Letters, vol. 2 (1), 2005
- [11] G. Krieger, N. Gebert, A. Moreira, *Multidimensional Waveform Encoding: A New Digital Beamforming Technique for Synthetic Aperture Radar Remote Sensing*, IEEE Trans. on Geoscience and Remote Sensing, in print, 2007.
- [12] G. Krieger, N. Gebert, A. Moreira, *Oral Presentation at IGARSS 2007*, Barcelona, Spain